Proton-boron fusion in a compact scheme of plasma oscillatory confinement

Yu. K. Kurilenkov [1,2,*], A. V. Oginov [2], V. P. Tarakanov [1], S. Yu. Gus'kov [2], and I. S. Samoylov [1]

[1] *Joint Institute for High Temperatures of the Russian Academy of Sciences, Izhorskaya 13 Building 2, Moscow 125412, Russia*
[2] *P.N. Lebedev Physical Institute of the Russian Academy of Sciences, Leninskii Ave. 53, Moscow 119991, Russia*

We present the results of experiments on the aneutronic fusion of proton-boron (pB) in a single miniature device with electrodynamic (oscillatory) plasma confinement. The device is based on a low energy ($\sim$1–2 J) nanosecond vacuum discharge with a virtual cathode, the field of which accelerates protons and boron ions to the energies required for pB synthesis ($\sim$100–300 keV) under oscillating ions' head-on collisions. The yields of α particles registered for different conditions of the experiment are presented and discussed in detail. The experiment was preceded by particle-in-cell modeling of main processes accompanying pB reaction within the framework of the full electromagnetic code KARAT. The summary yield of α particles of about $5 \times 10^4/4\pi$ was obtained during the pulse-periodic operation of the generator within total 4 μs of the high voltage applied, which is $\sim$10 α particles/ns.

I. INTRODUCTION

The aneutronic reaction of proton–boron (pB) fusion accompanied by the release of only three fast alpha particles, $p + {}^{11}\text{B} \rightarrow \alpha + {}^{8}\text{Be}^* \rightarrow 3\alpha + 8.7\,\text{MeV}$, is of great fundamental and applied interest, but requires extreme conditions for realization [1–3]. At present, there is a great deal of interest and progress in the use of proton-boron therapy in medicine [4,5]. Also, it is proposed to use fast α particles from the pB reaction to create jet thrust in space [6,7]. In the long term, the use of the pB aneutronic fusion could remove many of the difficulties of future nuclear power generation, associated with neutron radiation [8,9]. However, despite the great interest and discussion of various approaches to get really clean energy [8,10–12], the way to solve this problem is still far from being clear. In recent years, starting from Belyaev *et al.* experimented in 2005 [13], there has been an increased interest in the pB fusion reaction, and great progress has been achieved in α-particles yield in experiments with laser-driven pB fusion [14–16]. In experiments just with plasma confinement, without the action of external lasers or accelerators, the pB reaction has not yet been observed.

In fact, well-known schemes of magnetic or inertial confinement under operating temperatures like $T \sim 10$–20 keV [8] do not allow achieving pB reaction since the cross section is extremely small there [5,16]. The scheme of inertial electrostatic confinement (IEC) of plasma [9,17,18] turns out to be one of the few where, in principle, particle energies of $\geqslant 100$ keV can be achieved; starting from these energies the yield of the pB reaction becomes noticeable [16]. The acceleration and confinement of ions in the IEC scheme takes place in a deep electrostatic potential well (PW) [9,18]. In particular, to increase the efficiency of synthesis and avoid

the inefficient "beam-beam" scheme in a conventional IEC [9], it was proposed to inject electrons into the anode space to create PW, and proceed to the regime of periodically oscillating plasma spheres (POPS) [19,20]. In this advanced scheme, ions will undergo radial harmonic oscillations with any amplitude at the PW formed, and at the moments of maximal compression high fusion power have to be provided. However, despite the successful demonstration of the POPS scheme for H^{2+}, He^+, and Ne^+ [21], and its rather high efficiency predicted by theory [22], unfortunately, failed to implement the original POPS concept in further experiments on fusion [23]. Over time, it became clear that certain hopes associated with the potential advantages of POPS, including the favorable scaling of the fusion power, which increases with the inverse of the virtual cathode (VC) radius [19,21], can be realized in a IEC scheme with reverse polarity [18] based on nanosecond vacuum discharge (NVD) [24–27]. It involves automatic injection of electrons into the anode space when the high voltage is applied, and corresponding formation of a very small VC (with radius $r_{\text{VC}} \sim 0.1$ cm) and PW related (with depth $\varphi_{\text{PW}} \leqslant 100$ kV). Ions oscillate in the PW with a frequency of $\sim$80 MHz, registered in the experiment, reaching energies up to $\sim$100 keV at the moments of their head-on collisions at the PW bottom [26], where both DD synthesis [27] and aneutronic pB synthesis [28–30] have been observed. In fact, the field of VC keeps oscillating ions at potential well and simultaneously their inertia confines the electrons of VC by electric fields [9]. Thus, this type of confinement should be referred to as electrodynamic or oscillatory one.

This paper presents the results of the pioneering experiments on the aneutronic pB fusion in the field of a virtual cathode in a single miniature device with oscillatory confinement. The experiment was preceded by PiC modeling of main processes accompanying pB reaction [28,31] within the framework of the KARAT full electromagnetic code [32].
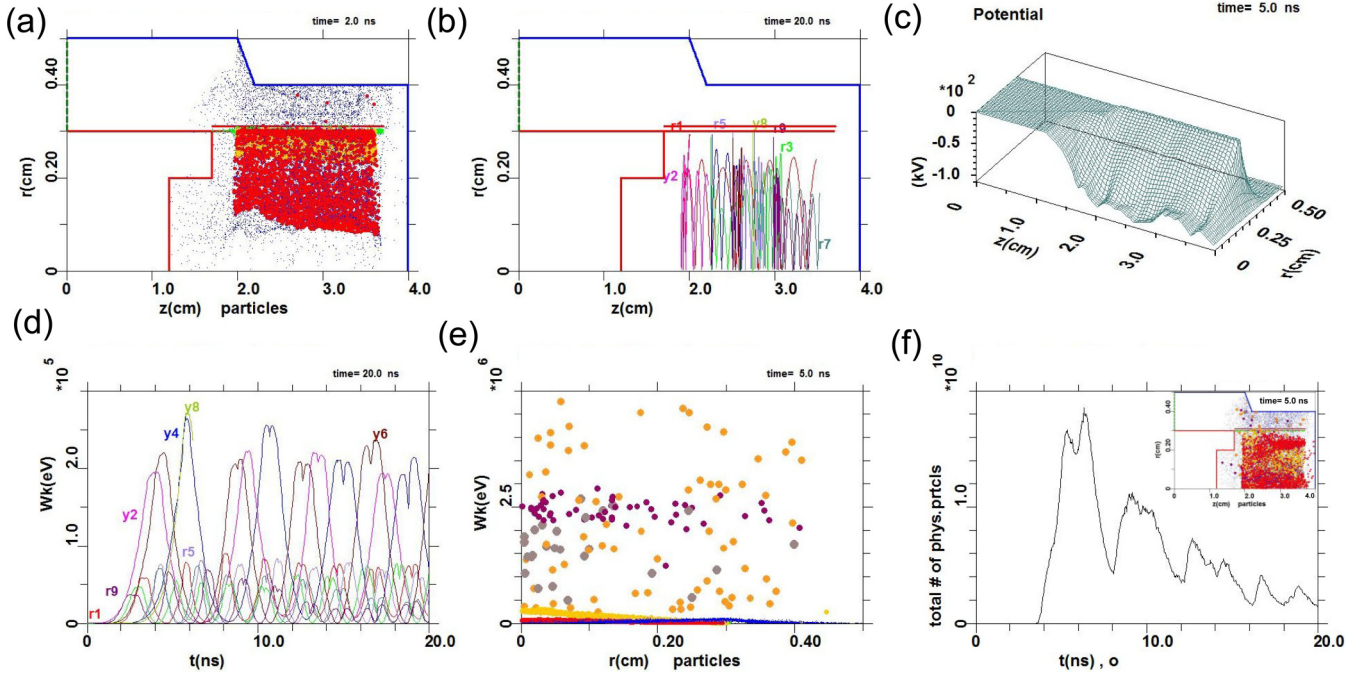
*yu.kurilenkov@lebedev.ru

FIG. 1. (a) Anode (red line)-cathode (blue line) geometry in the discharge gap where the virtual cathode is formed by electrons (blue points) at 2.0 ns, and protons (red) and boron ions (yellow) are accelerating in the potential well of the virtual cathode towards the Z axis where pB reaction should take place. The green area is simulated "erosion plasma" consisting of protons and boron ions. (b) Trajectories of particular groups of boron ions (y, $Z = +3$) and protons (r) during their oscillations around the axis Z. (c) Potential well of the virtual cathode as the possible micro-"reactor" for pB nuclear synthesis under oscillatory confinement. (d) Energy of groups of protons (r) and boron ions (y) as a function of time in the process of their oscillations in the potential well (at voltage applied $U = 100$ kV). (e) Energy of all particles participating in the nuclear pB reaction as a function of their position along the radius (blue points: electrons, yellow: boron ions, red: protons, gray: ^{8}Be*, purple: primary α-particles; dark orange: products of the ^{8}Be* decay into two secondary α-particles). (f) The yield of secondary α-particles (a.u.) from the ^{8}Be* decay during the pB reaction in nanosecond vacuum discharge. Inset illustrates pB reaction started with the yield of products at $t = 5$ ns [34].

II. ANEUTRONIC $p + {}^{11}$B FUSION SIMULATIONS: DESIGN OF EXPERIMENT

POPS-like oscillations of deuterons in the potential well of the virtual cathode followed by pulsating neutron yield (referred to as multiple fusion events) were recognized in early NVD experiments on DD fusion [24]. From standard IEC schemes with grid electrodes [9], we passed there to an oscillatory confinement scheme, which includes the key features of the strongly interdisciplinary physics of NVD with a hollow cathode [25,26]. The scheme, design, and description of this experiment are beyond the scope of this paper and given in detail elsewhere [25,27,33] (the main parameters of the discharge: $U = 70$–100 kV, $I_{max} \leqslant 2$ kA, $T_{pulse} \leqslant 50$ ns, total energy input about 1–2 J).

In the case of pB fusion, we also proceeded from the two-dimensional (2D) PiC modeling [28,29] to select and optimize the conditions of NVD experiment. An example of a PiC simulation of pB reaction at the discharge parameters close to actual operating ones in the experiment ($U = 100$ kV, $I = 1$–2 kA) is represented and discussed below in Figs. 1(a) to 1(f) (see [28] for principles and details of pB fusion 2D PiC simulations as well as Supplemental Material at [34] for KARAT simulation of the pB reaction video). Figure 1(a) (2 ns) illustrates how electrons (blue particles) are emitted from the cathode when voltage is applied, pass through the anode Pd

tubes area, and get into the axial region where are decelerated by the field of the formed VC. Then they are reflected and in part scattered. Positive particles of anodic "erosion plasma" (red: protons, yellow: boron ions) are drawn off by the field of VC and accelerated towards the Z axis. At the second ns, more light particles (protons) have moved closer to the axis than heavier ^{11}B ions [Fig. 1(a)]. By the fifth ns, boron ions have reached the Z axis and nuclear processes are initiated, accompanied by the yield of all the products of the pB reaction [Fig. 1(f), inset]. The particle yield by the fifth ns is presented in Fig. 1(e), where the energies and radial positions of electrons, protons, and boron ions, as well as beryllium and α-particles, are shown in the anode-cathode (A-C) space of the NVD (Here we used a well-established view of the pB reaction [35] with two low energy secondary α particles. A recent view [36] brings us back to the original one [2] that will change just Fig. 1(e)).

Instantaneous positions of the selected groups of boron ions and protons will correspond to their oscillations about the Z axis within the anode interior area [Fig. 1(b)] in the field of VC [Fig. 1(c)]. The temporal variation of the energies of the selected groups of protons and boron ions which are oscillating in the potential well [Fig. 1(c)] is shown in Fig. 1(d). Here, the energy of boron ions at the PW bottom is proportional to their charge chosen $Z = +3$. Probabilities of pB synthesis (and the corresponding α-particle yield) will
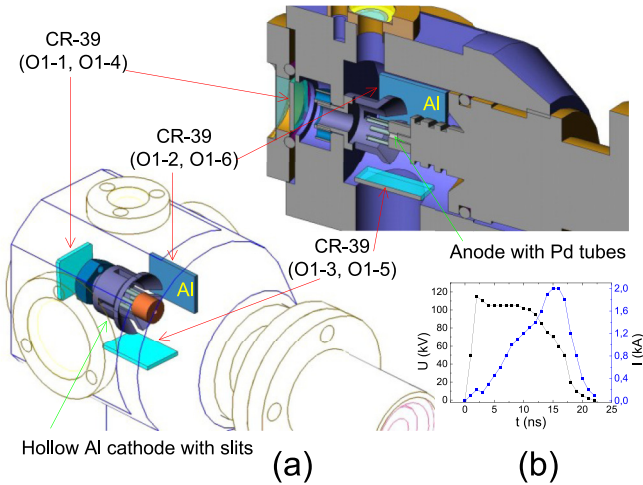
FIG. 2. (a) Sectional diagram of the discharge chamber and the arrangement of CR-39 detectors around the anode composed of Pd tubes and a hollow Al cathode with slits inside the chamber. (b) VA characteristics of the voltage pulse-periodical generator.

FIG. 3. (a, b) Boron nanoparticles deposited onto the developed anode surface by cataphoresis. (c) Microrelief of the Pd anode surface.

be increased sharply in certain points of "intersection" of the trajectories of protons and boron ions which are oscillating in the PW [Figs. 1(b) to 1(d)]. The corresponding example of secondary α-particle yield, arising from the beryllium decay, is presented in Fig. 1(f). The decay products of beryllium two α particles in its coordinate system have equal energies, but in the laboratory coordinate system they get different energies, which is observed in Fig. 1(e).

In the present work on the pB fusion reaction, a new hollow cathode with slits along the discharge axis was used in the cylindrical geometry of the NVD. It makes possible to observe the yield of α particles not only along the axis when registered from the hollow cathode end, but also along the discharge radius. The cylindrical anode with a copper base had six palladium tubes located perpendicular to the anode end along its perimeter. Figure 2(a) shows a schematic of a discharge chamber with an anode composed of Pd tubes and a cylindrical Al cathode inside, as well as its cross section (the entire chamber is no larger than a tennis ball in size). The volt-ampere characteristics of the employed voltage generator are shown in Fig. 2(b).

To register the α particles, track detectors CR-39 produced by the Fukuvi Chemical Industry company were used [37]. Their positions are shown in Fig. 2(a). At the end of the hollow cathode, there is a hole with a diameter of 4 mm through which high-energy particles can escape. The main part of the detectors is located at a certain distance behind the end of the hollow cathode to register the escaping protons, boron ions, and α particles along the discharge axis. Another part of the CR-39 detectors, both covered with an 11 μm Al foil and without foil, are located along the radius to register α particles that can escape in the radial direction through the slits in the cathode. Note that detectors covered with an Al foil will be capable of registering protons, boron ions, and α particles with energies $E_p > 0.9$ MeV, $E_{\text{Boron}} > 10$ MeV, and $E_\alpha > 3$ MeV, respectively. Calibration of the CR-39 detector by charged particles has been carried out on the beam of protons

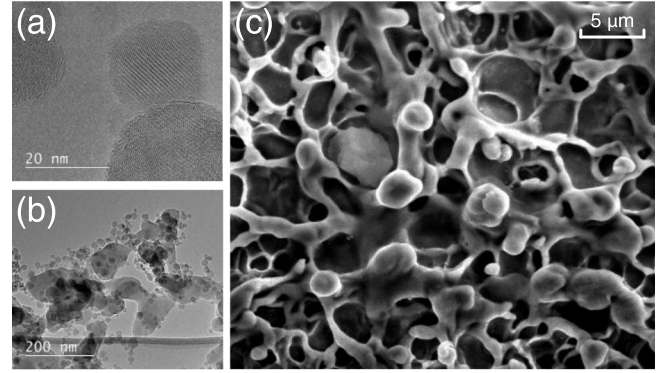from an electrostatic accelerator ($E_p = 0.5 - 3.0$ MeV), with standard α-sources ($E_\alpha = 2 - 7.7$ MeV). After the irradiation the detectors were etched in the solution 6M NaOH in H_2O at the temperature of 70 C for 2 hours. A procedure of the track detector calibration is considered in Ref. [38]. Tracks of boron ions identified in assumption of similarity with light ion tracks like Li, B, and C [39,40].

For pilot experiments on pB synthesis, an anode was chosen, which had previously been repeatedly used in experiments on DD synthesis [33]. Due to the long-term impulse action of high-energy electrons (up to 70 keV), Pd tubes of the anode have a developed surface with a huge number of microcraters [Fig. 3(c)]. Two modes of filling of the anode with hydrogen and boron were used. In the first case, the anode Pd tubes were saturated only with hydrogen by electrolysis in distilled water with the addition of sulfuric acid to ensure sufficient ionic conductivity of the electrolyte (this is the "background" version of the anode). Electrolysis was carried out at a current density of 10–20 mA/cm^2. In the second case, boron nanoparticles [Figs. 3(a) and 3(b)] were deposited on the surface of Pd anode tubes with a highly developed microrelief using cataphoresis in an aqueous suspension of boron nanopowders [41] (specific surface area $S = 80$ m^2/g, 50 ml of deionized water, 1 g of powder). In this case, in parallel with the process of the cataphoresis of boron nanoparticles, the volume of the anode Pd tubes was saturated with hydrogen also (similar to electrolysis in the "background" anode). The Pd anode filled with hydrogen from the inside and with boron outside was used in pB reaction experiment.

III. EXPERIMENTAL RESULTS: α-PARTICLES YIELD REGISTERED AND ESTIMATIONS RELATED

Let us start from radial observations, which are rather simple for interpretations. Figures 4(a) to 4(d) show the tracks on the CR-39 detector associated with charged particles that passed through the longitudinal slits along the radius of the cathode both for open detectors [Fig. 2(a) O1-3, O1-5] and for those covered with a 11 μm aluminum foil [Fig. 2(a) O1-2, O1-6]; the width of the cathode slits is 0.2 cm. For the CR-39 detector both with and without the foil, a feature of the radial yield of particles observed is the presence of tracks associated
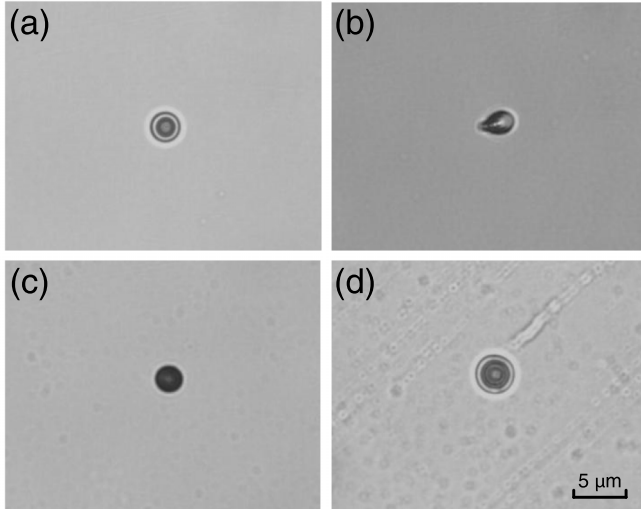
FIG. 4. Tracks on the CR-39 detector associated with α-particles that passed through the longitudinal slits along the radius of the cathode: (a, b) for detectors O1-6 covered with 11 μm Al foil, (c, d) for open detectors O1-5.

FIG. 5. Examples of microphotographs of the surface of the CR-39 detector: (a) for discharges with a "background" anode containing only hydrogen (there are tracks of protons only); (b) for the discharge with an anode saturated with hydrogen and covered with boron nanoparticles (tracks of protons, boron ions, and α-particles are visible), where (c)–(f) are enlarged fragments of the images of the O1-4 detector: Panels (c, d) are open detectors, (e, f) are CR-39 covered by Al foil.

with α particles only. This can be explained by the fact that the potential well [Fig. 1(c)] is deep enough, and confine almost all protons and boron ions oscillating at PW along the radius [Figs. 1(b) and 1(d)]. Indeed, in the process of oscillations, charged particles reach maximum energies corresponding to just about 80% of the potential well depth [Fig. 1(d)]. As a result, only high-energy α particles leave PW in radial direction and escape through the cathode slits in both cases. In addition, it is seen that the difference in the track areas for the foil-covered CR-39 detector [Fig. 4(a) and 4(b)] and open detectors [Fig. 4(c) and 4(d)] is small. Apparently, though the flight of an α particle through the foil filters decreases its energy, the track areas corresponding to the 2–4 MeV energy range may vary within the limits close to the measurement error (see, for example, Fig. 5 in Ref. [39]).

The general picture of tracks registered by open CR-39 detectors for particles flying along axis Z through hollow cathode looks more complex. Figures 5(a) to 5(f) show typical examples of microphotographs of the surface of the track detectors [Fig. 2(a) O1-1, O1-4] both for discharges for a "background" anode containing only hydrogen (a) and for the anode saturated with hydrogen and boron nanoparticles (b)–(f) (in Figs. 5(a) and 5(b) area 120 by 90 μm of CR-39 detector is shown). In the first case [Fig. 2(a), O1-1], naturally, only tracks of protons were registered [Fig. 5(a)]. In the second case (O1-4), protons, boron ions, and individual α particles have appearing on the detector. Further, Figs. 5(c) and 5(d) represent particular α-particle tracks (O1-4) under better resolution. The tracks attributed to α particles were placed in the central region of the detector front surface selected for analysis. For reliable identifying of registered tracks, the limited number of control shots were performed with detector CR-39 covered by Al foil [Figs. 5(e) and 5(f)].

For a quantitative analysis of the tracks, Fig. 6 shows histogram of track areas for shots with an anode with hydrogen and boron. It can be seen that alongside with the proton tracks,
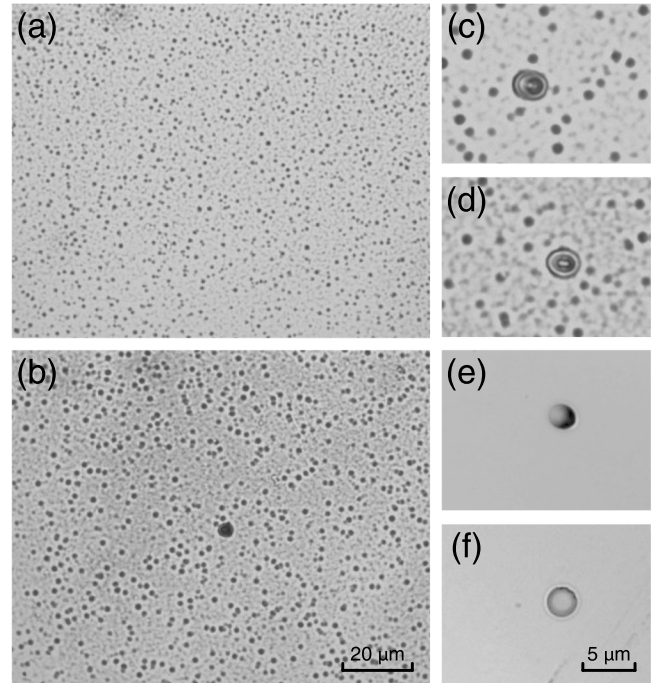
with a characteristic area of about or less than 1 μm^2 [like in Fig. 5(a)], there is a second maximum in the region of about 2 μm^2 attributed to accelerated along axis Z [Fig. 1(c)] boron ions. Remark, the diameters of these tracks ($\leqslant$2 μm) corresponds to available data on boron, lithium, and carbon ions CR-39 tracks [39,40], extrapolated on boron ions energies ($\leqslant$300 keV) and etching time 2 hours in our experiment. The peak around 17 μm^2 [Fig. 5(b)] is ascribed to α particles with energy 4.1 $\pm$ 0.3 MeV [39] since it coincides completely with tracks on Al covered detectors [Figs. 5(e) and 5(f)], where just α particles are registering [like in Figs. 4(a) and 4(b)]. For shots with a "background" anode, we observed in histogram similar to one presented in Fig. 6(a) just the tracks of protons [shown in Fig. 6(b)]. Thus, for shots with anode with hydrogen and boron we observe through the hollow cathode [Fig. 5(b)] besides of protons the appearing of boron ions, accelerated by electric field along axis Z up to 100–300 keV, and very rare fast α particles from pB reaction. This conclusion confirms also by the using of CR-39 detectors covered by Al foil in the same experiment, where just similar α-particles tracks were registered [Figs. 5(e) and 5(f)] like in Fig. 5(b).

The quantitative results on registration of the yield of α particles in the pilot experiments are summarized in Table I [CR-39 indexes and positions are shown in Fig. 2(a)]. The first row refers to the experiment with the boron-free anode. Since there is no escape of α particles, the right column
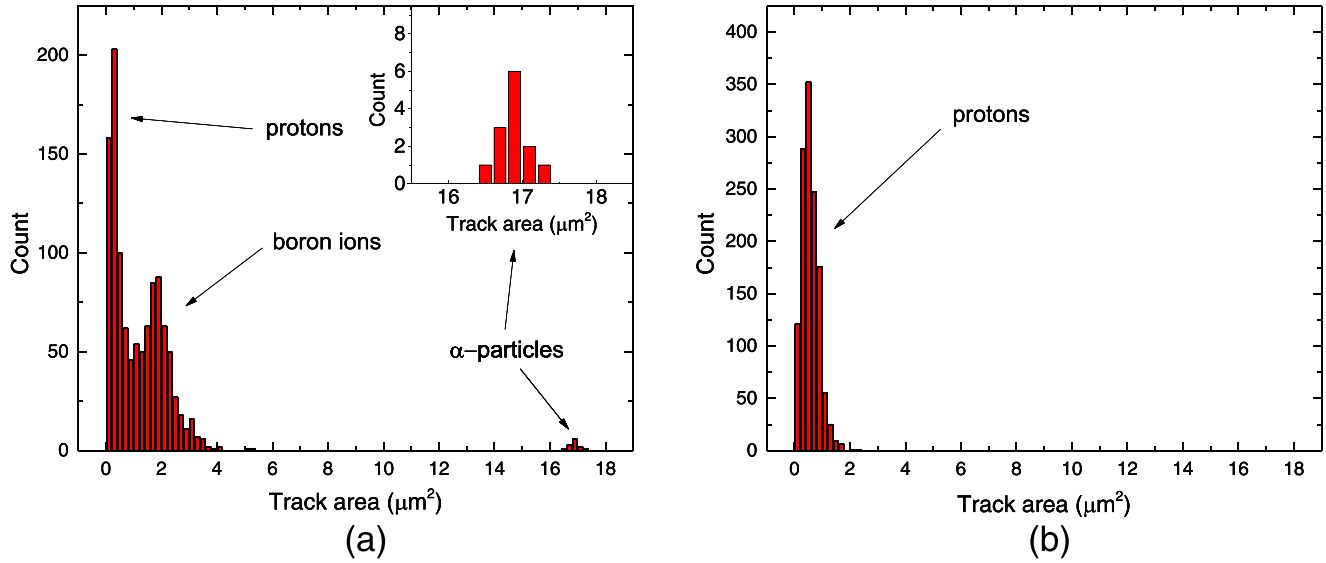
FIG. 6. (a) Histogram of track areas obtained in experiments under hydrogen-filled anode with boron [Fig. 5(b)]. (b) Similar histogram for shots with hydrogen-filled anode without boron [Fig. 5(a)] has just a proton peak.

contains just the "natural" number of tracks available on the CR-39 detector before its use (about 40). The second row corresponds to the experiment with a hydrogen-filled anode with boron. In this experiment, the registered number of new tracks of α particles (about 160) is four times larger than the "natural" values, and in fact, characterizes the real aneutronic pB synthesis in our oscillatory confinement scheme. The next four rows in Table I correspond to the registration of the escape of α particles in the radial direction. The obtained values of the number of tracks (168 and 92), at first glance, correspond to a smaller excess over the "natural" level than for observations with the end-on detector. But, note, the later value of the total number of tracks (92) was obtained with such an arrangement of the tubular anode, when one of the anode Pd tubes partially screened the side slit in the cathode for α particles flying from the discharge axis along the radius, and thus was prevented partially their escape. Also, note, the tracks number $168 - 53 = 115$ registered for detector O1-6 [Fig. 2(a) and Table I] corresponds to 2/3 of total number of α particles generated in the pB reaction since the low energy α particles (~ 1 MeV [36]) will not pass through the foil, but can be registered by an open detector [like in Fig. 4(d)].

The total track densities given in Table I were obtained for approximately 200 voltage pulses. Note that in the experiment described, the geometry of the treated Pd anode with

a developed microrelief was not yet optimal for achieving a well-defined ions oscillations and corresponding high-yield pB reaction related. Therefore, the obtained results on the yield of α particles are still qualitative. Nevertheless, in the approximation of the isotropic yield of α particles, it can be estimated that approximately a $5 \times 10^4/4\pi$ yield of α particles was obtained during the repetitively pulsed operation of the voltage generator for about $4\,\mu$s, which is on average about $250\,\alpha$ particles per one shot or about $10\,\alpha$ particles/ns in a given series of experiments. Let us note that the energies of protons ($\leqslant 100$ keV) and boron ions ($\leqslant 300$ keV) in the NVD [Fig. 1(d)] are relatively small, for example, in comparison with those in the laser-driven proton-boron fusion [16], and efficiency $Q = E_{\text{output}}/E_{\text{input}}$ in the experiment is still very low $\sim 10^{-10}$–10^{-9}. Nevertheless, the noted ion energies make it possible to use partially the known resonance of the reaction pB cross section in the vicinity of 162 keV to increase the yield of α particles [3,5,16]. Also, if to increase the voltage up to $U = 150$ kV or higher, we can get closer to the main resonance peak of pB reaction at 675 keV.

Let us estimate the α particles yield in the present experiment assuming that the main yield will be determined by only one single convergence to discharge axis of head-on accelerated protons and boron ions ($Z = +3$) up to maximum of energies 100 keV and 300 keV, correspondingly.

TABLE I. Results of α particles tracks measurement by CR-39 detectors ("natural" density of α-particle tracks is near 40–50 cm^{-2}).

CR-39 index	Discharge conditions (anode filling)	Covering of CR-39	Distance from discharge zone, mm	Density of α particles, cm^{-2}
O1-1 end-on	Hydrogen	No Al foil	15–18	40
O1-4 end-on	Hydrogen + boron	No Al foil	15–18	200
O1-2 side	Hydrogen	Al (11 μm)	12	53
O1-6 side	Hydrogen + boron	Al (11 μm)	12	168
O1-3 side	Hydrogen	No Al foil	12	45
O1-5 side	Hydrogen + boron	No Al foil	12	92

Approximately, it is illustrated in Fig. 1(d) by head-on collision of group $r5$ of protons with boron ions group $y8$, near the sixth ns of the simulation. Then, the α particles yield can be expressed as $N_\alpha \approx (1/2) n_p^{\text{comp}} \cdot n_B^{\text{comp}} \cdot \tau_{\text{comp}} \Omega_{\text{min}} \langle \sigma v \rangle$, where $n_p^{\text{comp}} = N_{0(p)}/\Omega_{\text{min}}$ and $n_B^{\text{comp}} = N_{0(B)}/\Omega_{\text{min}}$ is the density of compressed protons and borons at the axis, correspondingly, $N_{0(p)}$ and $N_{0(B)}$ are the total values of protons and borons in anode space, τ_{comp} is the time of noticeable pB reaction under particles collapse at the axis, Ω_{min} is the volume of the pB reaction, σ is the cross-section of the pB reaction, v is the velocity of the center of mass ($\approx 1.6 \times 10^8$ cm/s). The estimate of the total particles' densities as $N_{0(B)} \approx N_{0(p)} \approx I\tau/e(Z_B + 1) \approx 3 \times 10^{13}$ ($I = 1$ kA, time of voltage applied $t = 20$ ns, e is the charge of the electron), and take the cylindrical volume of the pB reaction as $\Omega_{\text{min}} = \pi R^2 L \approx 3.9 \times 10^{-3}$ cm^3 (volume length $L \approx 0.5$ cm, $R \approx 0.05$ cm). If to take the cross section in the interval $\sigma = 10^{-3}$–10^{-2} barn, we have $N_\alpha \approx 18$–180, correspondingly. The resonance peak at 162 keV with $\sigma \approx 0.1$ barn looks rather narrow [3,5,8], and its role is unlikely to exceed 10–20%. For the case of a larger number of well-defined oscillations of ions [27] during time of pulse τ in a better geometry of electrodes [like in Fig. 1(d)], we obtain at least $N_\alpha \sim 10^3$ α particles per shot.

Notably, our cylindrical NVD device is rather different from those originally designed for POPS [19–21], and we avoid here some restrictions caused by the particle convergence in the spherical geometry [23,42]. Apparently, in the cylindrical geometry, the POPS-like oscillations in our steady-state plasmas are mainly the mechanism of resonant heating of ions rather than the mechanism of coherent compression, as it in the original POPS concept [19]. As remarked in Ref. [23] (Sec. V), unlike in the standard POPS scheme, it may be possible to use the resonant heating for ions of different masses, in particular, for the proton-boron advanced fuel [28] as done in our experiment.

IV. CONCLUSION

The aneutronic synthesis of proton-boron in a single miniature device with electrodynamic (oscillatory) plasma confinement based on a low energy ($\sim$1–2 J) nanosecond vacuum discharge is demonstrated, and the results of the registration of the yield of α particles are presented. In fact, when a pulsed voltage (100–120 kV) is applied, beams of high-energy autoelectrons interact with the hydrogen-filled Pd anode covered with boron, and form complex near-surface erosion plasma containing protons and boron ions. The subsequent acceleration of ions by the field of the virtual cathode and head-on collisions of some part of protons and boron ions with energies of the order of 100–300 keV in the process of their oscillations in the potential well lead to the pB reaction, which is evidenced by the detection of generated α particles. Further studies are to show the prospects for the creation of a practical compact reactor on aneutronic pB synthesis with non-Maxwellian plasma [27,42,43], based on the oscillatory confinement presented. If the latter endeavor is successful, then in a number of future applications [9,21], including propulsion [6,7], the good power-to-weight ratio in our device may also be useful.

[1] M. L. E. Oliphant and E. Rutherford, Proc. R. Soc. London A **141**, 259 (1933).

[2] P. I. Dee and C. Gilbert, Proc. R. Soc. London A **154**, 279 (1936).

[3] W. Nevins and R. Swain, Nucl. Fusion **40**, 865 (2000).

[4] D.-K. Yoon, J.-Y. Jung, and T. S. Suh, Appl. Phys. Lett. **105**, 223507 (2014).

[5] G. Cirrone, L. Manti, D. Margarone, G. Petringa, L. Giuffrida, A. Minopoli, A. Picciotto, G. Russo, F. Cammarata, P. Pisciotta *et al.*, Sci. Rep. **8**, 1141 (2018).

[6] C. Ohlandt, T. Kammash, and K. G. Powell, in *AIP Conference Proceedings*, Vol. 654 (American Institute of Physics, Melville, NY, 2003), pp. 490–496.

[7] A. Krishnamurthy, G. Chen, P. Keutelian, B. Ulmen, and G. Miley, in *AIAA SPACE 2012 Conference & Exposition* (AIAA, Reston, VA, 2012), p. 5146.

[8] S. Atzeni and J. Meyer-ter Vehn, *The Physics of Inertial Fusion: BeamPlasma Interaction, Hydrodynamics, Hot Dense Matter*, Vol. 125 (Oxford University Press, Oxford, 2004).

[9] G. H. Miley and S. K. Murali, *Inertial Electrostatic Confinement (IEC) Fusion Fundamentals and Applications* (Springer, NY, 2014).

[10] D. C. Moreau, Nucl. Fusion **17**, 13 (1977).

[11] N. Rostoker, A. Qerushi, and M. Binderbauer, J. Fusion Energy **22**, 83 (2003).

[12] H. Hora, S. Eliezer, G. Kirchhoff, N. Nissim, J. Wang, P. Lalousis, Y. Xu, G. Miley, J. Martinez-Val, W. McKenzie *et al.*, Laser Part. Beams **35**, 730 (2017).

[13] V. S. Belyaev, A. P. Matafonov, V. I. Vinogradov, V. P. Krainov, V. S. Lisitsa, A. S. Roussetski, G. N. Ignatyev, and V. P. Andrianov, Phys. Rev. E **72**, 026406 (2005).

[14] C. Labaune, C. Baccou, S. Depierreux, C. Goyon, C. Loisel, V. Yahia, and J. Rafelski, Nat. Commun. **4**, 2506 (2013).

[15] A. Picciotto, D. Margarone, A. Velyhan, P. Bellutti, J. Krasa, A. Szydlowsky, G. Bertuccio, Y. Shi, A. Mangione, J. Prokupek *et al.*, Phys. Rev. X **4**, 031030 (2014).

[16] L. Giuffrida, F. Belloni, D. Margarone, G. Petringa, G. Milluzzo, V. Scuderi, A. Velyhan, M. Rosinski, A. Picciotto, M. Kucharik *et al.*, Phys. Rev. E **101**, 013204 (2020).

[17] O. A. Lavrent'ev, Ann. NY Acad. Sci. **251**, 152 (1975).

[18] W. C. Elmore, J. L. Tuck, and K. M. Watson, Phys. Fluids **2**, 239 (1959).

[19] R. A. Nebel and D. C. Barnes, Fusion Technol. **34**, 28 (1998).

[20] D. Barnes and R. Nebel, Phys. Plasmas **5**, 2498 (1998).

[21] J. Park, R. A. Nebel, S. Stange, and S. K. Murali, Phys. Rev. Lett. **95**, 015003 (2005).

[22] L. Chacon, G. Miley, D. Barnes, and D. Knoll, Phys. Plasmas **7**, 4547 (2000).

[23] E. Evstatiev, R. Nebel, L. Chacon, J. Park, and G. Lapenta, Phys. Plasmas **14**, 042701 (2007).

[24] Yu. K. Kurilenkov, M. Skowronek, and J. Dufty, J. Phys. A: Math. Gen. **39**, 4375 (2006).

[25] Yu. K. Kurilenkov, V. Tarakanov, M. Skowronek, S. Yu. Guskov, and J. Dufty, J. Phys. A: Math. Theor. **42**, 214041 (2009).

[26] Yu. K. Kurilenkov, V. Tarakanov, and S. Yu. Gus'kov, Plasma Phys. Rep. **36**, 1227 (2010).

[27] Yu. K. Kurilenkov, V. Tarakanov, S. Yu. Gus'kov, A. Oginov, and V. Karpukhin, Contrib. Plasma Phys. **58**, 952 (2018).

[28] Yu. K. Kurilenkov, V. Tarakanov, and S. Yu. Gus'kov, J. Phys.: Conf. Ser. **774**, 012133 (2016).

[29] Yu. K. Kurilenkov, S. Yu. Gus' kov, and V. P. Tarakanov, in *The Book of Abstracts: 10th Int. Conf. on Inertial Fusion Sciences and Applications (IFSA2017), September 11–15, Saint Malo, France* (ILP, CNRS, Saint Malo, 2017), P.Tu. 46.

[30] Yu. K. Kurilenkov, A. V. Oginov, V. Tarakanov, S. Yu. Gus' kov, I. S. Samoylov, V. E. Ostashev, and V. T. Karpukhin, in *Book of Abstracts of the XLVI International Zvenigorod Conference on Plasma Physics and Controlled Fusion, March 18–22* (GPI RAS–PLASMAIOFAN, Moscow, 2019), p. 126.

[31] Yu. K. Kurilenkov, V. Tarakanov, S. Yu. Gus' kov, I. S. Samoylov, and V. E. Ostashev, J. Phys.: Conf. Ser. **653**, 012026 (2015).

[32] V. Tarakanov, EPJ Web Conf. **149**, 04024 (2017).

[33] Yu. K. Kurilenkov, V. Tarakanov, S. Yu. Guskov, V. Karpukhin, and V. Valyano, Contrib. Plasma Phys. **51**, 427 (2011).

[34] See Supplemental Material at http://link.aps.org/supplemental/10.1103/PhysRevE.103.043208 for KARAT simulation of pB reaction, video.

[35] H. Becker, C. Rolfs, and H. Trautvetter, Z. Phys. A - Atomic Nuclei **327**, 341 (1987).

[36] S. Stave, M. Ahmed, R. France III, S. Henshaw, B. Müller, B. Perdue, R. Prior, M. Spraker, and H. Weller, Phys. Lett. B **696**, 26 (2011).

[37] V. S. Belyaev, A. P. Matafonov, V. P. Krainov, A. Y. Kedrov, B. V. Zagreev, A. S. Roussetski, N. G. Borisenko, A. I. Gromov, A. V. Lobanov, and V. S. Lisitsa, Nucl. Phys. (in Russian) **83**, 370 (2020).

[38] V. Belyaev, V. Vinogradov, A. Matafonov, S. Rybakov, V. Krainov, V. Lisitsa, V. Andrianov, G. Ignatiev, V. Bushuev, A. Gromov *et al.*, Phys. At. Nucl. **72**, 1077 (2009).

[39] C. Baccou, V. Yahia, S. Depierreux, C. Neuville, C. Goyon, F. Consoli, R. De Angelis, J. Ducret, G. Boutoux, J. Rafelski *et al.*, Rev. Sci. Instrum. **86**, 083307 (2015).

[40] J. Zhu, L. Chadderton, D. Fink, S. Cruz, S. Ghosh, and D. Zhu, Nucl. Instrum. Methods Phys. Res., Sect. B **105**, 208 (1995).

[41] F. Booth, J. Chem. Phys. **18**, 1361 (1950).

[42] S. Yu. Gus'kov and Yu. K. Kurilenkov, J. Phys.: Conf. Ser. **774**, 012132 (2016).

[43] R. L. Hirsch, in *14th U.S.-Japan IECF Workshop, Maryland USA, October 14–17* (2012), http://www.aero.umd.edu/sedwick/posters.html.